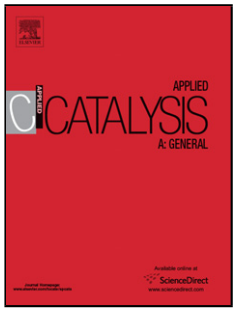

Title: Multicomponent $NiSnCeO_2$/C catalysts for the low-temperature glycerol steam reforming

Author: L. Pastor-Pérez A. Sepúlveda-Escribano

PII: S0926-860X(16)30517-8
DOI: http://dx.doi.org/doi:10.1016/j.apcata.2016.10.022
Reference: APCATA 16038

To appear in: *Applied Catalysis A: General*

Received date: 5-5-2016
Revised date: 14-10-2016
Accepted date: 21-10-2016

Please cite this article as: L.Pastor-Pérez, A.Sepúlveda-Escribano, Multicomponent NiSnCeO2/C catalysts for the low-temperature glycerol steam reforming, Applied Catalysis A, General http://dx.doi.org/10.1016/j.apcata.2016.10.022

Multicomponent $NiSnCeO_2$/C catalysts for the low-temperature glycerol steam reforming

L. Pastor-Pérez and A. Sepúlveda-Escribano*

Laboratorio de Materiales Avanzados, Departamento de Química Inorgánica - Instituto Universitario de Materiales de Alicante, Universidad de Alicante, Apartado 99, E-03080 Alicante, Spain.

*Corresponding author: asepul@ua.es

Graphical abstract

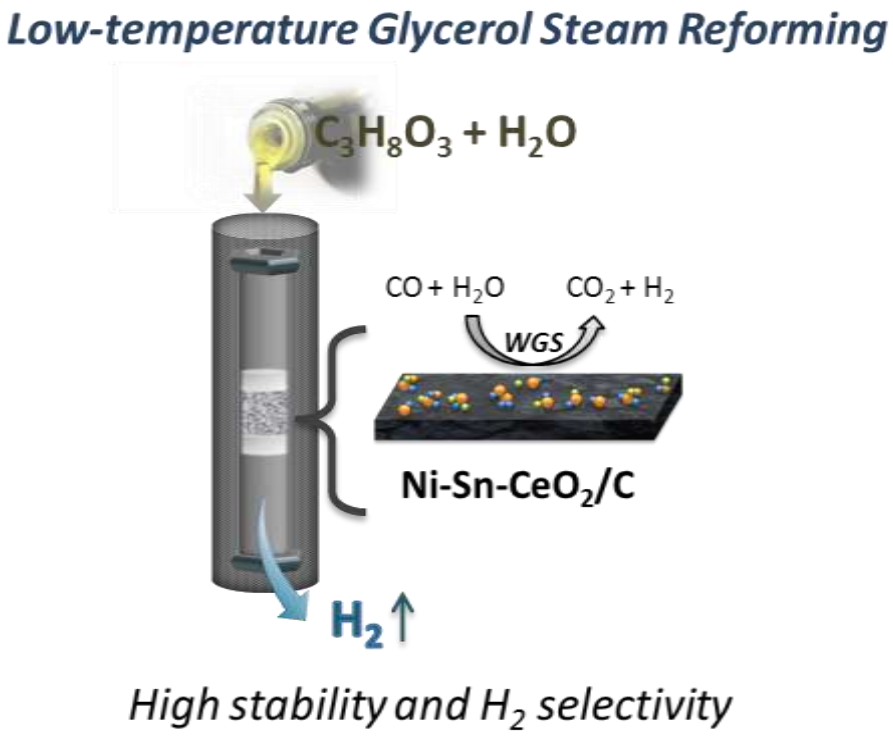

HIGHLIGHTS

- Ceria-promoted Ni-Sn catalysts supported on carbon are active in low temperature glycerol steam reforming.
- CeO_2 dispersed on carbon enhances the water-gas shift reaction, thus promoting the selectivity towards hydrogen.
- Formation of a Ni-Sn alloy mitigates Ni sintering and improves catalyst's stability.

Abstract

In this work, the low-temperature hydrogen production via glycerol steam reforming over activated carbon-supported Ni and Ni-Sn catalysts promoted by ceria was studied. A combination of N_2 adsorption, powder X-ray diffraction, temperature-programmed reduction with H_2, X-ray photoelectron spectroscopy and TEM analysis were used to characterise the Ni-Sn-CeO_2 interactions and the CeO_2 dispersion over the activated carbon support. The catalytic activity results show that the presence of ceria enhances the water-gas shift reaction, thus promoting the selectivity towards hydrogen. The inclusion of Sn stresses the influence of ceria in the displayed performance. Moreover, the

formation of a Ni-Sn alloy seems to be an efficient way to mitigate Ni sintering and therefore to improve the overall catalyst's stability.

Keywords: H_2 production, Nickel-tin, Glycerol, Ceria, Activated carbon

1. Introduction

Developing ways to utilise more effectively the abundant and renewable biomass resources available should be imperative nowadays. This provides new sources of energy and chemical intermediates, diminishing both the petroleum society dependence and its consequent global warming effect [1]. The use of biomass as raw material to produce hydrogen or synthesis gas is an interesting alternative route because it is renewable and its CO_2 emissions are almost neutral [2].

Among the multiple sources of biomass, the low-value glycerol that is produced as a waste in biodiesel synthesis from the transesterification of vegetable oils and animal fats is an interesting feedstock to be upgraded [3]. The production levels of biodiesel are increasing constantly; therefore, finding a profitable outcome to waste glycerol solutions can lower the manufacture costs of biodiesel [4].

Typically, glycerol is converted to more valuable products through reforming reactions [5]. In this sense, steam reforming of glycerol is one of the most common routes. However, this process is rather endothermic and normally requires elevated temperatures in order to obtain high performances. Alternatively, glycerol steam reforming to produce H_2 rich streams or H_2/CO mixtures can be performed at relatively low temperatures over metal-based catalysts in the so-called low-temperature steam reforming. This approach improves the economic viability of the process, allowing the efficient combination of the endothermic conversions of glycerol with the exothermic following steps in a hypothetical integrated process (water-gas shift, Fischer-Tropsch or methanol synthesis). At the same time, the low-temperature steam reforming imposes some challenges in the catalyst design that have to be covered.

On the other hand, the catalytic conversion of polyols to H_2, CO and CO_2 involves the preferential cleavage of C-C bonds as opposed to C-O bonds [1], being Pt-based

catalysts the most effective system for this process. Indeed, we have recently demonstrated the suitability of monometallic and bimetallic systems based on Pt and Pt-Sn supported on carbon for glycerol upgrading [6]. In particular, the presence of Sn benefits the catalyst's stability allowing higher glycerol conversions during long term periods. Furthermore, carbon supports seem to be a good choice since they are not able to catalyse dehydration reactions, due to their relatively inert chemical nature under reaction conditions, while exhibiting an excellent performance in the reforming of aqueous glycerol solutions when combined with a metallic active phase [7, 8].

Although Pt-based catalysts are more active in terms of specific activity, we propose in this paper Ni as a potential candidate to replace Pt from the bimetallic metal-Sn ensemble, since this transition metal represents a rather cheaper alternative with good skills for reforming processes [9]. Furthermore, the addition of Sn is reported to avoid alkane formation by the methanation reaction over metallic Ni. However, the catalytic activity of Ni-based catalysts is not modified by adding Sn [10 ,11]. On the other hand, the formation of nickel carbide has been proposed as the initial step of coke formation. The similar electronic structure of carbon and elements of groups IV and V (Ge, Sn, Pb, etc.) may favour the interaction of these metals (free *p* electrons) with Ni 3*d* electrons, thereby reducing the chance of nickel carbide formation [12, 13]

And not least, the presence of an active support/promoter as ceria provides several interesting advantages for a reforming catalyst. Its well-known activity in the WGS reaction enriches hydrogen concentration in the reformate gas and reduces carbon monoxide formation [14]. In addition, the excellent redox properties of this rare earth oxide improve the redox reversibility of the metallic phase [15], and the basic character of ceria mitigates coke formation, which is usually due to dehydration reaction taking place in the catalyst´s acid sites [16]. Moreover, ceria dispersion on a high surface carrier as activated carbon potentiates its catalytic skills, allowing to obtain smaller oxide nanoparticles and higher oxygen mobility while reducing the metal oxide spending [17]

In this way, a series of multicomponent NiSn/CeO_2/C catalysts for hydrogen production via glycerol reforming is proposed. One of the aims of this work is to prepare optimised Ni-CeO_2 catalysts, reducing the amount of ceria, in which the interaction between the metal and the oxide is enhanced, thus improving the catalytic activity. The reaction is carried out at relatively low temperatures and the catalytic performance is

compared to that of Sn-free $NiCeO_2/C$ systems. The effect of Sn on the activity, stability and physicochemical properties of the catalysts is also a subject of this study.

2. Experimental

2.1 Catalysts preparation

The procedure used for the synthesis of the catalysts was similar to that reported in our previous work [18]. The support was an industrial activated carbon (RGC30, from Westvaco). This carbon was ground and meshed (300-500 μm). The corresponding amount of $Ce(NO_3)_3 \cdot 6H_2O$ (99.99%, Sigma–Aldrich) to obtain 20, 30 and 40 wt.% of CeO_2 was dissolved in acetone. Dried carbon was added to the solution, in a proportion of 10 $mL \cdot g^{-1}_{support}$, with stirring. After 12 h, the excess of solvent was slowly removed under vacuum at 40 ºC, and the solid was then dried in the oven overnight. Finally, the dried solid was heat treated for 4 h at 350 ºC under flowing He (50 $mL \cdot min^{-1}$), with a heating rate of 1 $ºC \cdot min^{-1}$, in order to slowly decompose the cerium nitrate to form CeO_2, and trying to avoid the modification of the carbon surface by the evolved nitrogen oxides [19].Three CeO_2/C samples were prepared with different nominal CeO_2 loadings: 20, 30 and 40 wt.%.

Nickel addition to the CeO_2/C solid was carried out using the proper amount of $Ni(NO_3)_2 \cdot 6H_2O$ (99.9%, Sigma-Aldrich) in acetone to obtain 15 wt.% Ni, using 10 mL of solution per gram of solid. After stirring for 12 h, the solvent was removed under vacuum at 40 ºC. Finally the solid was treated at 350 ºC for 4 h under flowing He (50 $mL \cdot min^{-1}$). For the sake of comparison, Ni/C and Ni/CeO_2 catalysts were also synthesised. The ceria support was prepared by homogeneous precipitation from an aqueous solution of $Ce(NO_3)_3 \cdot 6H_2O$ (99.99%, Sigma-Aldrich) containing an excess of urea. The solution was heated at 80 ºC and kept at this temperature, with slow stirring, during 12 h. The solid formed was filtered and calcined at 350 ºC for 4 h. The CeO_2 support prepared in this way was impregnated with the Ni precursor as described for the carbon supported catalysts. In this way, five samples were prepared, which were labelled as Ni/C, $Ni20CeO_2/C$, $Ni30CeO_2/C$, $Ni40CeO_2/C$ and Ni/CeO_2.

In addition, Ni-Sn catalysts were prepared by sequential impregnation. Tin addition to the dried $NiCeO_2/C$ samples was carried out using the proper amount of $SnCl_2$ (99%, Sigma-Aldrich) dissolved in acetone (10 mL of solution per gram of solid) to obtain catalysts with a Ni:Sn atomic ratio of 10:1. After stirring for 12 h, the solvent was removed under vacuum at 40 ºC. Five tin-containing catalysts were prepared, which were labelled as NiSn/C, $NiSn20CeO_2/C$, $NiSn30CeO_2/C$, $NiSn40CeO_2/C$ and $NiSn/CeO_2$.

2.2. Catalysts characterisation

The textural properties of the supports were characterised by nitrogen adsorption measurements at -196°C. Gas adsorption experiments were performed in a home-made fully automated manometric equipment. Prior to the adsorption experiments, samples were out-gassed under vacuum (10^{-4} Pa) at 150 °C for 4 h. The specific surface area was estimated after application of the BET equation.

X-Ray powder diffraction patterns were recorded on a Bruker D8-Advance with a Göebel mirror and a Kristalloflex K 760-80 F X-Ray generation system, fitted with a Cu cathode and a Ni filter. Spectra were registered between 20 and 80° (2θ) with a step of 0.05° and a time per step of 3 seconds.

Temperature-programmed reduction (TPR) with H_2 measurements were carried out with the calcined catalysts in a U-shaped quartz cell using a 5% H_2/He gas flow of 50 $mL \cdot min^{-1}$, with a heating rate of 10 $°C \cdot min^{-1}$. Hydrogen consumption was followed by on-line mass spectrometry (Pfeiffer, OmniStar GSD 301). CuO standard (99.999%) was employed for the TPR calibration.

X-Ray photoelectron spectroscopy (XPS) analyses were performed with a VG Microtech Multilab 3000 spectrometer equipped with a hemispherical electron analyser and a Mg-Kα (h = 1253.6 eV; 1 eV = $1.6302 \cdot 10^{-19}$ J) 300-W X-ray source. The powder samples were pressed into small Inox cylinders. Before recording the spectra, the samples were maintained in the analysis chamber until a residual pressure of ca. $5 \cdot 10^{-7}$ $N \cdot m^{-2}$ was reached. The spectra were collected at pass energy of 50 eV. The intensities were estimated by calculating the integral of each peak, after subtracting the S-shaped background, and by fitting the experimental curve to a combination of Lorentzian (30%)

and Gaussian (70%) lines. The binding energy (BE) of the C l s peak of the support at 284.9 eV was taken as an internal standard. The accuracy of the BE values is ± 0.2 eV.

2.3 Catalytic tests

The catalytic behaviour of the prepared catalysts in the glycerol steam reforming reaction was evaluated under mild reaction conditions in a fixed bed reactor (Microactivity Refererence). Prior to the activity tests, catalysts were *in-situ* reduced under 50 mL·min^{-1} of H_2 at 350 ºC during 2 h. From the process perspective, the activation process at 350 ºC permits a direct heat integration (reaction/activation) avoiding extra costs on heat exchange. The reaction was carried out for 30 h, at atmospheric pressure and 350 ºC, with a feeding (0.05 mL·min^{-1}) containing 10 w/w glycerol in water. Activity tests were performed using 0.200 g of catalyst diluted with SiC, to avoid thermal effects. The composition of the gas stream exiting the reactor was determined by gas chromatography (Agilent Technologies), with two columns (Carboxen-1000 and Porapak-Q) and two detectors (FID and TCD).

The catalytic performance was evaluated in terms of conversion into gaseous products (based on a carbon balance between the inlet and the outlet of the reactor), selectivity to main reaction products (where "i" is CO_2, CO and CH_4) and also hydrogen yield, which were defined as:

$$\%\,\text{Conversion} = \frac{\text{C in the gas products}}{\text{C fed into reactor}} \cdot 100$$

$$\%\,\text{"i" selectivity} = \frac{\text{"i" produced experimentally}}{\text{C atoms in the gas products}} \cdot 100$$

$$\%\,H_2\,\text{Yield} = \frac{H_2\ \text{produced experimentally}}{H_2\,\text{calculated according to Eq (1)}} \cdot 100$$

Eq. 1 is the glycerol steam reforming reaction**:**

$$C_3H_8O_3\,(g) + 3H_2O\,(g) \rightarrow 3CO_2\,(g) + 7H_2\,(g) \qquad \text{(Eq.1)}$$

3. Results and discussion

3.1 Textural properties

Table 1 shows the specific surface area (N_2, -196 °C, BET), the micropore volume (V_{micro}, N_2, -196 °C, D-R) and the volume of mesopores (V_{meso}) for the prepared samples and the parent carbon support. The textural parameters of bulk ceria are also included for sake of comparison.

The N_2 adsorption isotherms at -196 °C for all the carbon-based materials (not shown) correspond to a combination of Type I and Type IV isotherms, which are characteristic of materials containing both micro- and mesopores. In fact, the mesoporous volume is always slightly larger than the microporous one. Data in Table 1 show a continuous decrease of the BET surface area for the Ni-ceria-loaded carbons as the amount of ceria increases, and the same trend is observed for both the micropore and the mesopore volumes. This effect has been previously reported [19] and it is partially attributed to the blockage of porosity by Ni and ceria crystallites to a certain extent. It has also to be taken into consideration that ceria addition decreases the textural parameters of these materials, as compared with those of the parent Ni/C, as an effect of the increase of mass and the much lower porosity of ceria as compared with carbon. The nearly lineal decrease of the textural parameters with increasing the ceria content indicates that this effect has a more important contribution.

It has to be noted the much lower surface area of the ceria support and of the ceria-supported nickel catalyst as compared to that their carbon-supported counterparts.

The impregnation stage with the tin precursor also produces a smooth decrease in the BET surface area of the catalysts, which is also attributed to the presence of Sn in low concentration.

3.2 H_2-temperature-programmed reduction

Temperature programmed reduction studies were conducted in order to assess the redox properties of the catalysts and to analyse the interaction between the different metallic species and the support. Fig. 1 shows the H_2-TRP profiles of the prepared materials. The profile obtained with the Ni/C catalyst presents two peaks at low and

medium temperatures, respectively. The first peak, centred at 240 ºC, is ascribed to the reduction of small and well dispersed nickel oxide particles, while the peak at higher temperature accounts for the reduction of medium size NiOx species, as described elsewhere [18]. For the Ni/CeO_2 catalyst two reduction zones were observed. The low temperature one, between 150 and 400 ºC, is related to the reduction of NiOx particles in contact with ceria and also to the surface reduction of ceria, while the peak at high temperatures (700-900 ºC) is due to the bulk ceria reduction normally observed in this temperature range [20]. The ternary $NiCeO_2/C$ systems show intermediate redox behaviour with both NiO_x and CeO_2 contributions. More specifically, three reduction processes were observed in the H_2-TPR profiles for $NixCeO_2/C$. The first low temperature peak is attributed to the reduction of highly dispersed NiO on the support, and the intermediate ones correspond to the surface reduction of ceria with different degree of interaction with nickel particles. Several types of Ni species coexist depending of the Ni/Ce ratios. In addition, for solids with higher ceria loadings, Ni-Ce solid solution and well dispersed NiO phase may coexist, as has been reported before [21, 22]

The addition of Sn provokes notable changes in the TPR profiles. All the samples show a more homogeneous reduction profile with overlapping of the main reduction processes: nickel, tin and ceria species reduction. Ni-Sn interaction is evidenced by the delay on NiO reduction. It seems that Sn stabilises highly dispersed NiOx species shifting the reduction process towards higher temperatures. This stabilising effect subsequently influences ceria reduction, that is shifted towards lower temperatures due to an enhanced hydrogen spillover effect on the stabilised nickel particles. Regarding Sn, it is well established that tin reduction may happen in a wide range of temperatures strongly depending on the support. For instance, reduction of massive Ni-Sn Raney catalysts takes place at around (260 ºC) [27] while the reduction of a bimetallic Ni-Sn supported on Al_2O_3 happens at 450 ºC [27]. In this work, the authors report that the samples were composed of a mixture of Ni_3Sn, metallic tin and SnOx. In our case, the reduction of tin species overlaps with the simultaneous reductions of NiOx and CeO_2 happening between 300-450 ºC. The lower reduction temperature observed in our study is related to the weak interaction of the active species with the carbon support [19].

Overall, the multicomponent nature of the studied catalysts makes it difficult to accurately assign the different reduction processes, but it seems clear that the addition of tin modulates the redox behaviour of the prepared materials. Therefore, in order to extract

further information from the TPR experiments, the total reducibility was calculated for each sample. The reducibility percentage was calculated from the integrated area of reduction peaks. The theoretical H_2 consumption was calculated considering complete reduction of Ni, Sn, the chloride precursor for tin deposition and the Ce^{4+}/Ce^{3+} process. This theoretical value was referred to the experimental one value obtained from the TPR calibration, and the percentage of reducibility was obtained from the equation below.

% Reducibility = Experimental H_2 consumption/ Theoretical H_2 consumption • 100

(Eq. 2)

Table 1 shows the calculated values. It is clear that the carbon-supported catalysts present much higher reducibility that the massive samples, Ni/CeO_2 and $NiSn/CeO_2$. Among the carbon-supported samples, the ceria containing catalysts are slightly less reducible, with a clear trend showing that the reducibility decreases upon increasing ceria loading. Very importantly, the addition of tin boosts the reducibility for all the studied samples, indicating the impact of tin in the redox properties of these materials.

3.3 XPS characterisation of reduced catalysts

Further insights on the chemical modifications of the catalysts after reduction in H_2 at 350 ºC were investigated by XPS. The samples were reduced *ex-situ* and conserved in octane until the analysis. The binding energies (B.E.) of the main peaks of the Ni $2p_{3/2}$ and Sn $3d_{5/2}$ energy levels are summarised in Table 2, and selected XPS spectra are presented in Fig. 2. In the absence of tin, the reduced catalysts exhibited complex Ni $2p_{3/2}$ spectra (Fig. 2A), pointing to the presence of different nickel species. For instance, the band at *ca.* 852.6 eV is assigned to metallic Ni^0 species, while the bands at about 854.7 and 856 eV are ascribed to NiO and $Ni(OH)_2$ species, respectively [23, 24]. The presence of ceria shifts the Ni^{2+} bands towards higher binding energies, what indicates a strong Ni-CeO_2 interaction in good agreement with the TPR data. This interaction may modify the structure and electronic properties of Ni, this enhancing the catalytic behaviour of these materials [25]. In any case, it should be mentioned that Ni was not completely reduced in any of the samples after the reduction treatment.

The situation is more complex for the tin containing samples. Table 2 summarises the positions (binding energies) of the Sn $3d_{5/2}$ XPS bands observed for the Sn-doped samples. This band is constituted by two contributions as shown in Fig. 2B. The peak centred at *ca.* 485 eV is attributed to Sn^0 while the peak centred at 486.4 eV is related to oxidised tin species [11]. It is worth mentioning that the presence of metallic Sn can be associated to the formation of a Ni-Sn alloy, as pure tin oxide is known to reduce only at above 527 ºC [26]. Indeed, Shabaker et al. demonstrated, by using Mossbauer spectroscopy, the presence of Ni_3Sn after a reduction treatment similar to that employed this work [27]. In fact, and according to our Ni/Sn atomic ratio, Ni_3Sn is the possible alloy when the Ni-Sn phase diagram is considered [28].

Furthermore, tin addition also modifies the Ni XPS features. In particular, the presence of Sn promotes Ni reducibility leading to a higher concentration of metallic Ni species (calculated values shown in Table 2). This observation agrees with the redox features discussed in the TPR section (see for instance the reducibility values in Table 1) and underlines the intimate Ni-Sn contact. The presence of reduced Sn and Ni can be linked to the above mentioned formation of a Ni-Sn alloy. However it is rather difficult to distinguish by XPS whether the reduced tin and nickel species are isolated or included in the Ni-Sn alloy. Indeed, Ni XPS spectra with and without tin shown in Fig. 2A are very similar and just a slight shift of the Ni bands could be intended. In any case, the Ni-Sn interaction is evident and correlates well with the results obtained in the TPR experiments. In fact, this Ni-Sn contact is also influenced by the presence of ceria and its loading. In this sense, it must be underlined that 30 wt.% of CeO_2 seems to be the optimal loading to provide an adequate environment facilitating the chemical interactions among the active phase and the promoters. As shown in Table 2, $NiSn30CeO_2/C$ is the catalyst with the highest concentration of reduced Ni and with a rich proportion of Sn^0. Also, the $NiSn20CeO_2/C$ catalyst presents the richest Sn^0 proportion in agreement with the TPR data (this is the ceria-based catalysts with the highest reducibility) and therefore, the Ni-Sn interaction should be favoured in this system.

3.4 XRD

Further insights on the chemical structure of the prepared samples were obtained by XRD analysis (Fig. 3A and 3B). Before measurements the samples were pre-reduced at 350 ºC, thus emulating the activation step before the glycerol reforming tests.

Some remarkable differences can be established between the studied catalysts. As a general trend, cerium oxide presents smaller particle sizes and higher amorphous character when supported on carbon. The typical fluorite cell reflexions are sharper and more intense for the ceria bulk materials compared to ceria supported on carbon. The later points a greater ceria dispersion, which is beneficial for the reforming reaction, and underlines the fact that better catalytic skills can be achieved with less amount of ceria if this oxide is dispersed in a high surface carrier as carbon. Similar results were obtained in recent works using ceria-based catalysts for WGS, with the oxide dispersed on an inert support [18, 29].

All the samples present the typical metallic Ni reflections accounting for the Ni reduction during the catalysts activation. Ni diffractions are more marked in the ceria-free samples, this indicating higher degree of crystallinity and bigger particle size of the Ni species in the absence of ceria. This is an interesting observation since, apparently, the ceria-free systems underwent stronger sintering during the activation. In other words, it seems that ceria mitigates to some extent metallic Ni agglomeration. It is well known that the oxygen vacancies present on ceria are electron rich sites where metallic particles preferentially nucleate [30]. This preferential nucleation of Ni on ceria's oxygen vacancies could explain the strong Ni-Ce interaction, which is evidenced also in the TPR profile, and accounts for the higher resistance of the ceria-containing materials to metal sintering.

The situation becomes more interesting when the NiSnXCeO_2/C series of catalysts are considered (Fig. 3B). Some peaks ascribed to Ni-Sn alloy were identified for the NiSn/C sample, in good agreement with the XPS data [31, 32]. In fact, the XRD data confirms that Ni-Sn alloy is formed during the activation process at 350 ºC and therefore, this relatively low activation temperature is enough to obtain the active catalyst´s configuration. The alloy diffraction peaks are more marked for the NiSn/C sample, once again evidencing the higher metallic dispersion and the smaller particle size of both the metallic Ni and the Ni-Sn alloy when ceria is present. This enhanced dispersion and the

smaller particle size of the active components could benefit the reforming performance in the ceria promoted catalysts.

3.5 Catalytic behaviour

The catalytic behaviour of the prepared multicomponent catalysts in terms of gas phase conversion as a function of time on stream, after being reduced at 350 ºC, is reported in Fig. 4. The steam reforming of glycerol was performed at atmospheric pressure, 350 ºC and 0.05 mL/min of a 10% w/w of aqueous glycerol solution. The reaction was carried out for 30 h in order to assess the deactivation process and to determine the effect of tin during these long reaction runs. The study of the catalytic stability is, from the industrial application point of view, as relevant as the catalytic activity. The gas phase analysis was carried out every 30 min by on line chromatography. A blank run with only the carbon support was also performed, and negligible glycerol conversion was obtained.

It can be seen in Fig. 4 that there is a clear effect of the ceria loading on the catalytic activity, being the sample containing 30 wt.% CeO_2 the most active one (Fig. 4A). Furthermore, in all cases, catalysts with CeO_2 were the most active materials. On the contrary, Ni/C shows a lower activity, this assessing the determinant role of ceria in this reaction due to its well-known redox properties, and also its ability to improve the stability and the catalytic performance of these catalysts by the synergistic effect between the Ni and CeO_2. The observed synergy is a cooperative effect which involves a close interaction among the active phases in such a way that each active component benefits from the other. In our case, Ni and CeO_2 are the active components, working synergistically to promote the reforming reaction. While Ni favours the C-C bond breaking, CeO_2 promotes the WGS reaction enhancing the selectivity towards hydrogen. In addition, ceria is vital to control Ni sintering while ceria needs Ni to overcome the WGS as reported elsewhere [18]. Therefore, one active phase needs the other one and vice versa, this resulting in an overall promotion of the activity.

On the other hand, two different activity windows can be distinguished. Firstly, at early reaction stages (less than 3 h), all the studied samples displayed good catalytic activity reaching high glycerol conversions. In this range most of the catalysts exhibit

comparable conversions, with the $NiSn30CeO_2/C$ sample outstanding among the others. This catalyst resulted to be the best one, reaching full alcohol conversion in the first 5 h on stream. From then on glycerol conversion progressively dropped for all the studied samples. Due to the complex nature of our catalysts, several factors might be responsible for the observed deactivation. In the simplest system, Ni/C, deactivation is mainly due to the sintering of metal particles. The absence of any other component (apart from the mere support) to stabilise and prevent Ni agglomeration leads to rapid Ni sintering, what explicates the activity depletion. In addition, C deposition is favoured in these agglomerated Ni particles, this also contributing to the deactivation. Fig. 5 shows TEM micrographs of the Ni/C and the $Ni30CeO_2/C$ catalysts, both fresh (just reduced) and spent, in order to clarify the catalysts deactivation phenomena. It can be seen that a considerable sintering of the metal particles has taken place in catalyst Ni/C (see Fig. 5C for the fresh and Fig. 5D for the used catalyst), when it is compared with catalyst $Ni30CeO_2/C$ (Fig. 5A and 5B for the fresh and the spent catalyst, respectively). Furthermore, the possibility of having coke covering the metal particles, although difficult to assess due to the carbonaceous nature of the carbon support, must be taken into account. It can be concluded that the presence of ceria slows down the agglomeration of the metallic particles. Indeed, the metallic sintering is considerably mitigated in all the ceria-containing catalysts, where only a slight increase in Ni particle size was detected. Even so, the ceria-supported Ni catalyst also experienced a relatively fast deactivation. A similarly quick deactivation was found by Dumesic et al. when basic supports were applied in the low-temperature glycerol reforming [7]. Apparently, the activity drop is caused by glycerol dehydration on the oxide catalyst support, which leads to the formation of carbonaceous blocking species that are accumulated on the surface [7, 33]. Very interestingly, the tin promoted materials seem to be less prone to deactivation. Despite the fact that the activity falls for all the tin-doped samples after 5 h on stream, this drop is smoother compared to that of the tin-free samples. It seems that tin allows greater glycerol conversion even when the catalyst is operating under deactivation conditions. The addition of Sn improves catalytic stability, avoiding Ni sintering, what is maybe due to the formation of Ni-Sn alloys.

The H_2/CO, CO/CO_2, CH_2/H_2 molar ratios for the product streams at 25 h on stream (when the steady state is reached) with $NixCeO_2/C$ and $NiSnCeO_2/C$ catalysts are summarised in Table 3. The stoichiometric H_2/CO ratio, if all glycerol were converted

into CO and H_2 ($C_3O_3H_8 \rightarrow 3CO + 4H_2$), is 1.3. In contrast, the H_2/CO ratios obtained over all samples were higher, this indicating a remarkable contribution from the water-gas shift reaction ($CO + H_2O \leftrightarrow H_2 + CO_2$). This behaviour is more clearly evidenced in the CO/CO_2 molar ratio, which is higher for Ni/C and NiSn/C (ceria-free samples). Therefore, it can be partially concluded that ceria benefits the hydrogen yield and influences the products distribution since its presence is linked to the WGS reaction [34].

The maximum H_2/CO ratio was obtained for samples containing 20 wt.% ceria, this suggesting a promoted WGS activity when ceria is dispersed over a high surface area carbon material, in good agreement with previous results [17]. This result also correlates well with the quantitative TPR analysis. In fact, 20 wt.% ceria leads to the highest reducibility within the ceria-containing catalysts, thus evidencing the direct correlation between the redox properties and the WGS reaction, as reported elsewhere [17]. For the Sn-containing samples a decrease of the H_2/CO ratio was obtained, which can be due to the presence of tin species blocking CeO_2 active sites. Furthermore, the CO/CO_2 molar ratio tends to increase with the presence of tin in the catalysts, this indicating that Sn slows down the WGS reaction in the multicomponent catalysts. On the other hand, the methanation reaction seems to have a minor influence in our process. Values for the CH_4/H_2 molar ratio in Table 3 show that methane formation remains low for all catalysts. Despite the presence of Cl traces (see Table 2), which could promote methanation, our catalysts are highly selective towards hydrogen production.

The H_2 yield and CO, CO_2, CH_4, CH_x selectivities are presented in Fig. 6. For all the ceria-containing catalysts (Fig. 6A), the H_2 yield and the selectivities to the different product are rather similar, independently of the ceria content. However, some pronounced differences were obtained upon tin addition. This change is more notorious for the $NiSn30CeO_2/C$ catalyst, which showed the best catalytic behaviour in terms of conversion and stability, and also reached a maximum H_2 yield of about 48 % (Fig. 6B). In this respect, the beneficial effect we have observed by adding Sn to the $Ni30CeO_2/C$ sample on the selectivity for H_2 production may be caused by the presence of Sn at Ni-defect sites, and by the formation of Ni-Sn surface alloy species, such a Ni_3Sn alloy, which maintain the high rates of C-C cleavage needed for H_2 production as reported by Dumesic´s group [11]. Furthermore, the best catalytic behaviour obtained with the $NiSn30CeO_2/C$ catalyst is in fair agreement with the characterisation data discussed above. This sample has enhanced reducibility and also, it is the one with a higher

concentration of reduced Ni and with a rich proportion of Sn^0, both metals synergistically interacting and thus favouring the catalytic performance. Also, 30 wt.% ceria provides a higher population of active sites which affect positively the catalytic behaviour. For the remaining NiSnxCeO$_2$/C samples a tendency was observed: CO_2 selectivity slightly increased with the amount of ceria while CO selectivity decreased, an effect that backs up the WGS contribution ascribed to ceria. Finally, tin addition affected to different extents the catalytic activity of these samples, blocking part of ceria active sites. Therefore, a larger amount of CeO_2 to increase the water-gas shift contribution is needed.

3.6 XRD post-reaction characterisation

Post-reaction characterisation provides some clues to support the catalytic activity discussion. Thus, XRD diffraction patterns of the spent catalysts are presented in Fig. 7. The XRD analysis confirms Ni sintering during the reforming reaction, especially for the NixCeO$_2$/C catalysts (the tin-free catalysts, Fig. 7A). Ni particle size is around 19 nm for all the samples presented in Fig. 7A, except for the Ni/C catalyst, whose Ni particle size is somewhat larger than *ca.* 23 nm (values estimated by the Scherrer equation). In the fresh (just reduced) samples (Fig. 3A) the particle sizes are smaller, typically around 12 nm for the ceria-containing catalysts and 18 nm for the Ni/C sample. This observation confirms the enhanced tolerance towards sintering exhibited by the ceria-based catalysts in fair agreement with the TEM results discussed above. In addition, some reflexions related to nickel oxide were found for the ceria-free samples. This situation reflects the higher stability of the alloy and the Ni particles when ceria is present, due to the preferential nucleation of these species on the oxygen vacancies of ceria.

Contrary to the NixCeO$_2$/C series (Fig. 7A), hardly visible peaks related to metallic Ni were observed for the multicomponent NiSnxCeO$_2$/C catalysts after reaction (Fig. 7B). Also, the peaks of the alloy phase are broader and smoother for these samples. This is a crucial difference between both series of catalysts, which reveals the absence of sintering of metallic particles when the Ni-Sn-Ce ensemble is considered. Shabaker *et al.* suggested that Sn migrates into the Ni particles to form Ni-Sn alloys during high-temperature reduction [27]. Indeed, diffusion of Sn into Ni occurs rapidly at elevated temperature, especially above the melting point of Sn (323 ºC) [35]. Therefore the use of Sn in the metallic phase has a strong effect on the catalytic properties of NiCeO$_2$/C solids.

The Ni-Sn alloy formed is better dispersed on the ceria-carbon support and, what is more important, it presents a higher tolerance to sintering in comparison with the monometallic $NiCeO_2$/C systems, this enhancing the catalytic behaviour in terms of larger hydrogen yields and stability with time on reaction.

4. Conclusions

We have developed a new family of ceria-promoted Ni and Ni-Sn catalysts supported on carbon for the low-temperature glycerol steam reforming. The multicomponent nature of the developed catalysts imposes a challenge when a fine correlation structure/activity is targeted, and further work is currently on-going in our group to tackle some unrevealed questions. However, some valuable remarks can be extracted from this work which certainly contributes to the debate on the glycerol steam reforming reaction.

In terms of the catalytic performance, our most active samples reached full glycerol conversion at early reaction stages with reasonably good hydrogen yields. In fact, hydrogen production is boosted via WGS due to the ability of ceria to carry out the shift process in the studied temperature window. Additionally, the strong influence of the WGS is reflected in the CO/CO_2 and the H_2/CO_2 ratios, in such a way that the obtained gas stream is rich in hydrogen and relatively poor in CO, an added value for further downstream processing.

For the tin-free catalysts, the catalytic activity is mainly related to the C-C bond breaking capacity of the Ni particles plus the WGS promotion associated to ceria. These catalysts are deactivated during continuous operation due to the sintering of Ni particles.

The inclusion of tin in the catalytic formulation leads to the formation of Ni-Sn alloy, an active phase in the glycerol reforming with better resistance towards sintering in comparison to the monometallic Ni system. For both the monometallic and the bimetallic systems, the presence of ceria improves the resistance to sintering to a certain extent. Furthermore, tin promotes the overall reducibility of the multicomponent catalysts thus enhancing the reforming skills.

Finally, it is worth noting that the active configuration of the catalysts (metallic Ni particles or Ni-Sn alloy supported on ceria-promoted carbon) can be achieved with a relatively smooth pre-activation treatment at 350 ºC. The perfect match between the reaction and the activation temperatures is an interesting advantage for the process integration in terms of heat exchange duties.

Acknowledgements

This work has been supported by Ministerio de Economía y Competitividad (Spain, project MAT2013-45008-P). L. P-P. acknowledges her grant BES-2011-0406508.

References

[1] R.D. Cortright, R.R. Davda, J.A. Dumesic, *Nature* 418 (2002) 964-967.

[2] A. Corma, S. Iborra, A. Velty, *Chem. Rev.* 107 (2007) 2411-2502.

[3] J.M. Encinar, J.F. González, A. Rodríguez-Reinares, *Ind. Eng. Chem. Res.* 44 (2005) 5491-5499.

[4] M.J. Hass, A.J. McAloon, W.C. Yee, T.A. Foglia, *Bioresour. Technol.* 97 (2006) 671-678.

[5] C. Len, R. Luque, *Sustain. Chem. Process.* 2:1 (2014) 1-10.

[6] L. Pastor-Pérez, A. Merlo, R. Buitrago-Sierra, M. Casella, A. Sepúlveda-Escribano, *J. Colloid Interface Sci.* 459 (2015) 160-166.

[7] R.R. Soares, D.A. Simonetti, J.A. Dumesic, *Angew. Chem. Int.* 45 (2006) 3982-3985.

[8] B. Kaya, S. Irmak, A. Hasanoglu, O. Erbatur, *Int. J. Hydrogen Energ.* 39 (2014) 10135-10140.

[9] R.R. Davda, J.W. Shabaker, G.W. Huber, R.D. Cortright, J.A. Dumesic, *Appl. Catal. B* 43 (2003) 13-26.

[10] G.W. Huber, J.W. Shabaker, J.A. Dumesic, *Science* 300 (2003) 2075-2078.

[11] J.W. Shabaker, D.A. Simonetti, R.D. Cortright, J.A. Dumesic, *J. Catal.* 231 (2005) 67-76.

[12] D.L. Trimm, *Catal. Today* 49 (1999) 3-10.

[13] L.F. Bobadilla, A. Penkova, F. Romero-Sarria, M.A. Centeno, J.A. Odriozola, *Int. J. Hydrogen Energ.* 39 (2014) 5704-5712.

[14] T.R. Reina, E. Papadopoulou, S. Palma, S. Ivanova, M.A. Centeno, T. Ioannides, J.A. Odriozola, *Appl. Catal. B* 150-151 (2014) 554-563.

[15] A. Iriondo, V.L. Barrio, J.F. Cambra, P.L. Arias, M.B. Guemez, M.C. Sanchez-Sanchez, R.M. Navarro, J.L.G. Fierro, *Int. J. Hydrogen Energ.* 35 (2010) 11622-11633.

[16] M. Ni, D.Y.C. Leung, M.K.H. Leung, *Int. J. Hydrogen Energ.* 32 (2007) 3238-3247.

[17] L. Pastor-Pérez, T.R. Reina, S. Ivanova, M.A. Centeno, J.A. Odriozola, A. Sepúlveda-Escribano, *Catalysts* 5(1) (2015) 298-309.

[18] L. Pastor-Pérez, R. Buitrago-Sierra, A. Sepúlveda-Escribano, *Int. J. Hydrogen Energ.* 39 (2014) 17589-17599.

[19] J.C. Serrano-Ruiz, E.V. Ramos-Fernández, J. Silvestre-Albero, A. Sepúlveda-Escribano, F. Rodríguez-Reinoso, *Mater. Res. Bull.* 43 (2008) 1850-1857.

[20] E. Van Ryneveld, A.S. Mahomed, P.S. Van Heerden, M.J. Green, H.B. Friedrich, *Green Chem.* 13 (2011) 1819-1827.

[21] M.M. Zyryanova, P.V. Snytnikov, R.V. Gulyaev, Y.I. Amosov, A.I. Boronin, V.A. Sobyanin, *Chem. Eng. J.* 238 (2014) 189-197.

[22] K. Chayakul, T. Srithanratana, S. Hengrasmee, *Catal. Today* 175 (2011) 420-429.

[23] J.H. Lin, V. Guliants, *ChemCatChem* 4 (2012) 1611-1621.

[24] I. Czekaj, F. Loviat, F. Raimondi, J. Wambach, S. Biollaz, A. Wokaun, *Appl. Catal. A* 329 (2007) 68-78.

[25] S.D. Senanayake, J.A. Rodriguez, D. Stacchiola, *J Phys. Chem. C* 116 (2012) 9544-9549.

[26] A. Onda, T. Komatsu, T. Yashima, J. Catal. 201 (2001) 13-21.

[27] J.W Shabaker, G.W Huber, J.A Dumesic, *J. Catal.* 222 (2004) 180-191.

[28] C. Xu, B.E. Koel, *Surface Sci.* 327, 1-2 (1995) 38-46.

[29] T.R. Reina, S. Ivanova, J.J. Delgado, I. Ivanov, V. Idakiev, T. Tabakova, M.A. Centeno, J.A. Odriozola, *ChemCatChem* 6 (2014) 1401-1409.

[30] C. Zhang, A. Michaelides, D.A. King, S.J. Jenkins, *J. Phys. Chem. C* 113(16) (2009) 6411-6417.

[31] V. Milanova, T. Petrov, O. Chauvet, I. Markova. *Rev. Adv. Mater. Sci.* 37 (2014) 42-47.

[32] M. Lu, Y. Tian, Y. Li, W. Li, X. Zheng, B. Huang, *Int. J. Electrochem. Sci.* 7 (2012) 760- 767.

[33] L.M. Martínez, T.M. Araque, J.C. Vargas, A.C. Roger, *Appl. Catal. B* 132-133 (2013) 499-510.

[34] A. Basinska, L. Kepinski, F. Domka, *Appl. Catal. A* 183 (1999) 143-153.

[35] M. Masai, K. Mori, H. Muramoto, T. Fujiwara, S. Ohnaka, *J. Catal.* 38 (1975) 128-134.

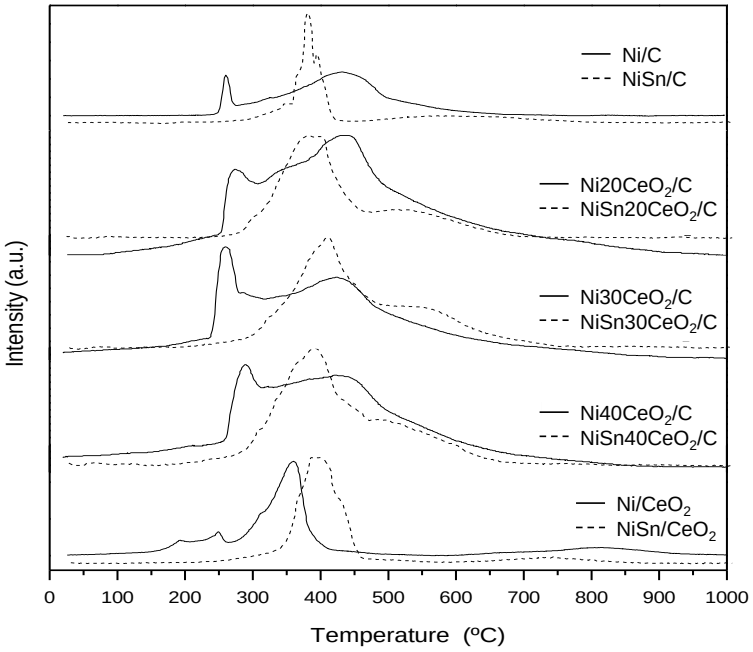

Figure 1. H_2-TPR profiles for $NiCeO_2/C$ (—) and $NiSnCeO_2/C$ (---) catalysts.

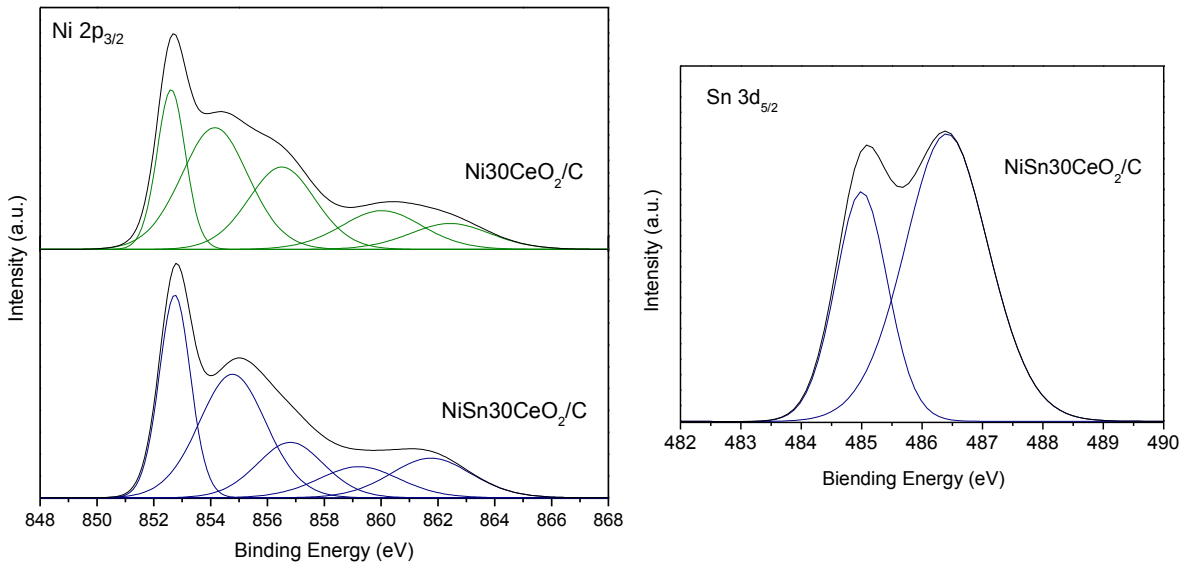

Figure 2. Selected XPS spectra of the studied samples: (A) Ni $2p_{3/2}$ region for $Ni30CeO_2/C$ and $NiSn30CeO_2/C$ catalysts and (B) Sn $3d_{5/3}$ region for $NiSn30CeO_2/C$ catalyst.

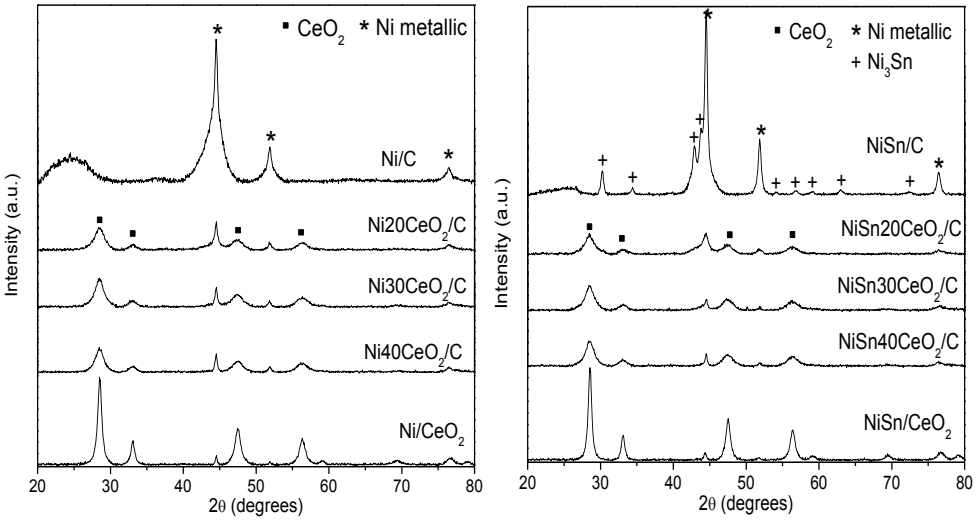

Figure 3. XRD characterisation for $NiCeO_2/C$ (A) and $NiSnCeO_2/C$ (B) catalysts reduced at 350 ^oC for 2 h.

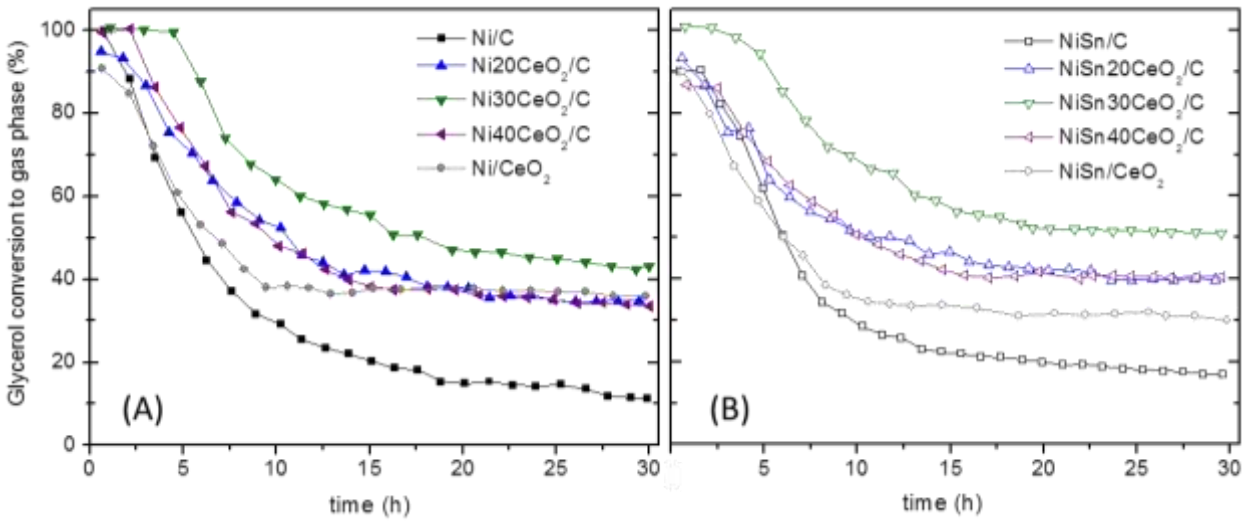

Figure 4. Gas phase conversion vs. time on stream for (A) $NiCeO_2/C$ catalysts and (B) $NiSnCeO_2/C$ catalysts in glycerol steam reforming at 350 ^oC.

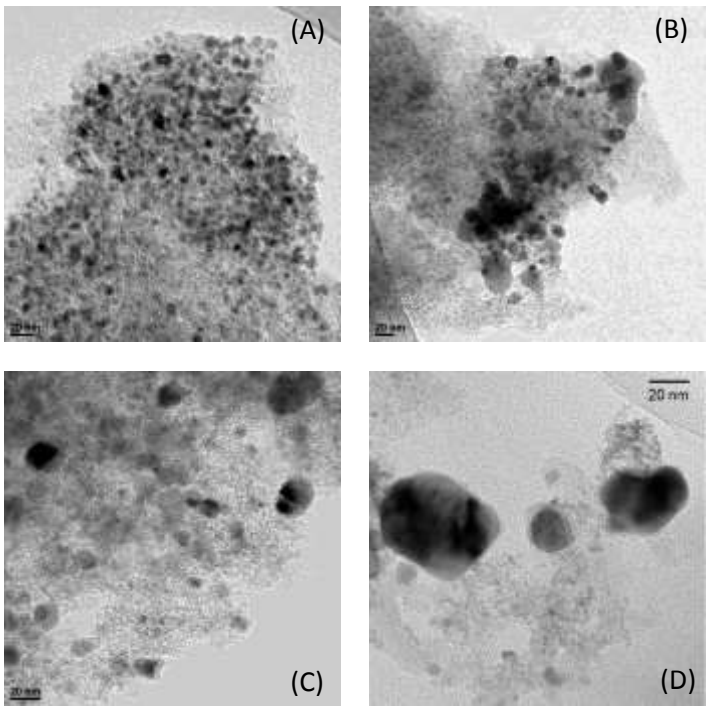

Figure 5. Selective TEM micrographs of $Ni30CeO_2/C$: (A) reduced and (B) spent; and Ni/C, (C) reduced and (D) spent (scale 20 nm).

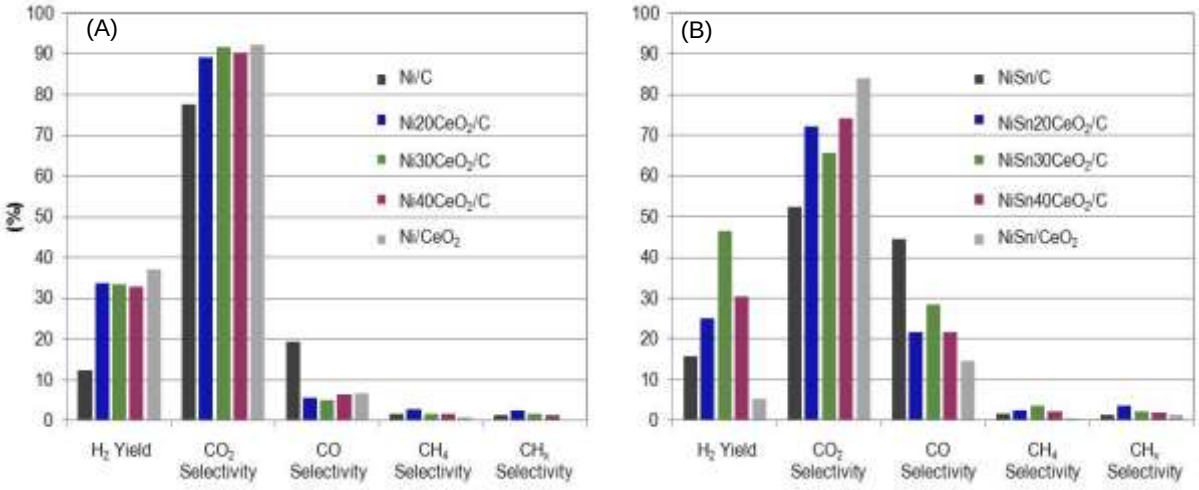

Figure 6. H_2 yield and selectivity for gas products in the GSR at 350 °C for $NiCeO_2/C$ (A) and $NiSnCeO_2/C$ (B) catalysts.

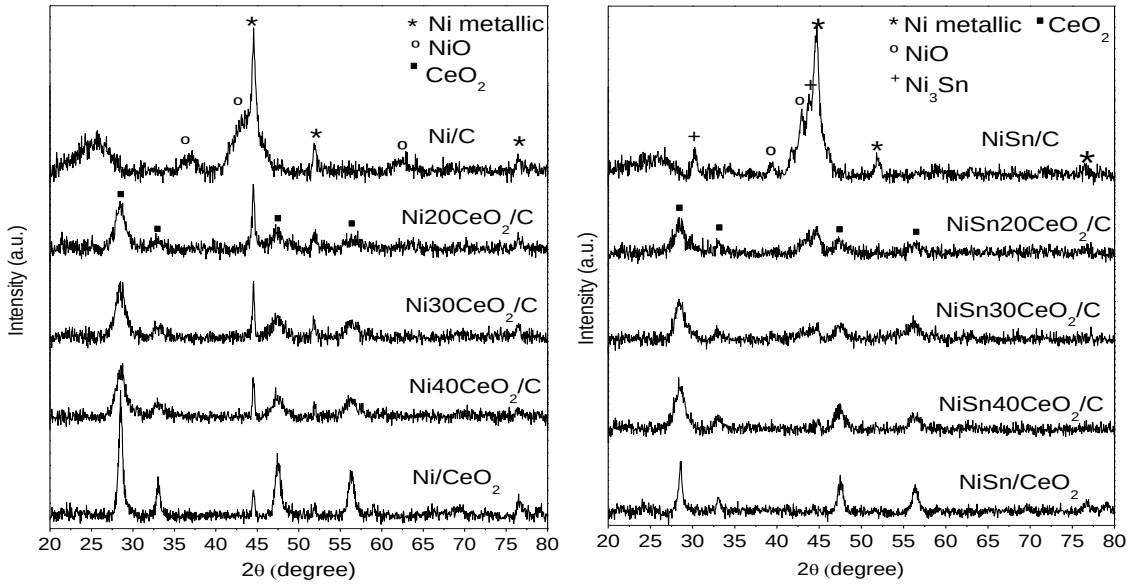

Figure 7. XRD post-reaction characterisation for $NiCeO_2/C$ (A) and $NiSnCeO_2/C$ (B) catalysts.

Table 1. Textural properties of supports and catalysts and reducibility of catalysts.

	$S_{BET}(m^2/g)$	$V_{micro}(cm^3/g)$	$V_{meso}(cm^3/g)$	*Reducibility (%)
C	1487	0.52	0.62	--
CeO_2	101	0.04	0.07	--
Ni/C	1238	0.45	0.52	83
Ni20CeO_2/C	807	0.28	0.34	65
Ni30CeO_2/C	677	0.23	0.28	62
Ni40CeO_2/C	512	0.19	0.21	59
Ni/CeO_2	70	0.03	0.04	13
NiSn/C	1228	0.41	0.52	86
NiSn20CeO_2/C	800	0.25	0.35	79
NiSn30CeO_2/C	676	0.23	0.29	70
NiSn40CeO_2/C	502	0.17	0.20	71
NiSn/CeO_2	69	0.02	0.03	33

*Calculated with Eq. 2.

Table 2. Binding energies of the Ni $2p_{3/2}$ and Sn $3d_{5/2}$ levels in catalysts reduced at 350 ºC.

Catalysts	**Ni $2p_{3/2}$ (eV)**		**Sn $3d_{5/2}$**	
	Ni^{2+}	**Ni^{0}**	**$Sn^{2+,4+}$**	**Sn^{0}**
Ni/C	854.1 - 856.3	852.3 (38)[1]	--	--
NiSn/C	854.1 - 856.2	852.8 (38)	486.4	484.9 (27)[1]
Ni20CeO_2/C	854.8 - 856.9	852.8 (33)	--	--
NiSn20CeO_2/C	854.8 - 856.6	852.9 (49)	486.4	485.0 (49)
Ni30CeO_2/C	854.2 - 856.5	852.6 (35)	--	--
NiSn30CeO_2/C	854.7 - 856.7	852.7 (55)	486.4	485.0 (33)
Ni40CeO_2/C	854.7 - 856.8	852.7 (35)	--	--
NiSn40CeO_2/C	855.2 - 857.2	853.0 (50)	486.7	485.6 (41)
Ni/CeO_2	855.4 - 857.6	853.6 (35)	--	--
NiSn/CeO_2	854.7 - 857.6	852.6 (51)	486.4	484.9 (16.5)

[1] Values in parenthesis indicate the percentage of metallic Ni and Sn calculated from XPS areas. Spectra of the Cl 2p region were also registered, but only traces of Cl (ca. 0.1% atomic) were obtained for all samples.

Table 3. Gas phase composition (molar ratios) and conversion in glycerol steam reforming at 350 ºC for all samples.

Catalyst	**H_2/CO**	**CO/CO_2**	**CH_4/H_2**	**Gas phase conv. (%)**
Ni/C	11.6	0.249	0.008	15
Ni20CeO_2/C	43.1	0.062	0.012	34
Ni30CeO_2/C	34.9	0.054	0.010	45
Ni40CeO_2/C	32.1	0.072	0.008	35
Ni/CeO_2	32.5	0.074	0.003	38
NiSn/C	5.6	0.849	0.006	18
NiSn20CeO_2/C	11.6	0.302	0.009	40
NiSn30CeO_2/C	9.4	0.479	0.016	52
NiSn40CeO_2/C	7.9	0.294	0.012	41
NiSn/CeO_2	12.9	0.173	0	26